Parameters identification of hot embossing machine based on the finite element method

Jun-yao Wang (153551490@qq.com)
Northeast Electric Power University
Qi Sun
Northeast Electric Power University
Bo You
Jilin University of Chemical Technology
Fu-wang Wang
Northeast Electric Power University

Original Article

Keywords: Hot embossing machine, Finite element method, Strength and stiffness, Thermal stress

Posted Date: April 7th, 2020

DOI: https://doi.org/10.21203/rs.3.rs-21198/v1

Title page

Parameters identification of hot embossing machine based on the finite element method

Jun-yao Wang, born in 1984. is currently a teacher in *school of mechanical engineering of Northeast Electric Power University*. He received his PhD degree from *Dalian Jiaotong Universityy, China*. His research interests include micro-nano fabrication and micro-nano fluids.

Tel: +86-15981176407; E-mail: 153551490@qq.com

Qi Sun, born in 1993, is currently a master candidate at *Northeast Electric Power University, China*. He received his bachelor degree from *Shandong University of Technology, China*, in 2017.
E-mail: 1171470526@qq.com

Bo You, born in 1983. is a teacher in *school of mechanical engineering of Jilin University of Chemical Technology*. He received his PhD degree from *Dalian Jiaotong Universityy, China*. His research interests include precision press fitting and automation of small parts.
F-mail:youbo198362@163.com

Fu-wang Wang, born in 1981, is a teacher in *school of mechanical engineering of Northeast Electric Power University*. He received his PhD degree from *Dalian Jiaotong Universityy, China*. His research interests include EEG robot.
E-mail: wangfuwangbaiyang@126.com

Corresponding author：Jun-yao Wang　E-mail：153551490@qq.com

ORIGINAL ARTICLE

Parameters identification of hot embossing machine based on the finite element method

Junyao Wang [1]• Qi Sun[1] • Bo You [2]• and Fu-wang Wang [1]

Abstract: A new type of hot embossing machine was developed, which comprised of frame structure and pressing head. To ensure fitting accuracy of the pressing heads, static simulation of columns as vertical moving guide was conducted, simulation results demonstrated that the column of the frame structure possessed enough stiffness via adopting the material of Q235 and the size of 30 mm, and the largest radial deformation of the column reached to 2.5nm. Thermoelectric refrigeration reactor (TRR) as the improved heating mode was utilized and the power was determined. Because the TRRs did not bear the whole pressing load, different types of pressing head are developed, which achieved the separation of pressing load and TRR's preload. Distributions of deformation on the feed direction were analysed for different types of pressing head. And simulation results demonstrated that the pressing head of "王" exhibited the best homogeneous deformation through comparing with other types of pressing head, which the maximum variation of deformation distribution approximately reached to 30nm. Additionally, force-thermal coupling simulation of pressing head plate as a core component was conducted to reduce thermal stress, and effects of distributions of deformation and temperature were discussed. For the given time, the head plate with the thickness of 18mm exhibited good uniformity of temperature and moderate heating rate, which the mentioned parameters reached 0.03°C/um^2 and 0.35°C/s, respectively. Generally, the applied thermal load decreases the deformation uniformity to a certain extent.

Keywords: Hot embossing machine • Finite element method • Strength and stiffness • Thermal stress

✉ Jun-yao Wang
153551490@qq.com

[1] School of Mechanical Engineering, Northeast Electric Power University, Jilin 132012, China

[2] School of Aeronautical Engineering, Ji Lin Institute of Chemical Technology, Jilin 132012, China

1 Introduction

With characteristic of low cost, a rapid reaction rate and high efficiency, microfluidic chip integrated highly into micro-units implemented the functions in aspects of DNA analysis, drug screening, cell manipulation and immunology determination [1-4]. Traditionally, microfluidic chips were fabricated with several materials including silicon, glass and polymer. Nevertheless, the applications for silicon and glass were limited due to low optical performance and small depth-width ratio respectively [5-6]. Fortunately, polymer materials represented by PMMA (polymethyl methacrylate) compensated for the former material's insufficiency, and demonstrated broad prospective with the characteristics of great varieties, low cost and easy mass production [7-9]. Remarkably, polymer materials were divided into thermosetting and thermoplastic. Comparing with the former, the thermoplastic possessed good performance of reprocess and recycle [10-12].

Currently, hot embossing machine for thermoplastic materials has been developed to manufacture the chip. Specifically, despite achieving the process of hot embossing, feeding accuracy didn't meet the requirements due to the use of early pneumatic drive [13-14]. With the development of electric motor, servo motor as the power was employed to improve the feeding accuracy of embossing machine. Nonetheless, an issue of demoulding difficulty was exposed on account of the adoption of air-cooling system. Simultaneously, influence of the air on chip was neglected during the fabrication process [15-16]. Fortunately, oil with large heat capacity was applied to boost the cooling rate. Furthermore, bubbles generation

was avoided through integrating a vacuum system. Nevertheless, thermal stress was increased owing to an integration design of resistance wire and water channels [17-18]. Particularly, TRR (thermoelectric refrigerator reactor) was installed to decrease thermal stress, which achieved the heating and cooling by the current reversing. Whereas two issues including low refrigeration efficiency and long processing cycle were emerged [19-20]. Dramatically, the mentioned issues were resolved with the assisted water tank. Because fitting precision for the pressing head was neglected, it was difficult to ensure accuracy of channel duplication of microfluidic chip[21-22]. Up to the point, the theoretical research on guaranteeing machining accuracy remains to need further development. Additionally, the mentioned foreign equipment were more expensive, and domestic equipment were not for sale.

In this paper, hot embossing machine composed of the frame structure and the pressing heads structure was established. To ensure the fitting accuracy of the pressing heads, static simulation of columns as vertical moving guide was conducted, radial stiffness of the column was studied in terms of material and size. The improved heating mode of TRR was utilized and the power was determined. Because the TRRs did not bear whole pressing load, the different types of head structures are developed, which achieved separation of pressing load and TRR's preload. Distributions of deformation on feeding direction were analysed. Additionally, to reduce thermal stress on accuracy of channel duplication of microfluidic chip, Force-thermal coupling simulation of pressing head plate as a core component was conducted, and effects of distributions of deformation and temperature were discussed. At the end of the article, the concluding remarks were demonstrated.

2 Theoretical basis for determining heat power

Considering low heating efficiency of traditional electric heating wire, TRRs comprised of Multiple P-N junctions were employed as heating/refrigerating element. Operating principle of single P-N junction included Seebeck effect, Parte effect, Thomson effect, Fourier effect and Joule effect[23-24]. Through analyzing the mentioned principle, Refrigeration capacity (Q_C) and heating capacity (Q_H) of the single P-N junction were respectively derived, as shown in Eqs. (1), (2). And parameters were shown in the following table 1.

$$Q_C = (\alpha_p - a_N) I T_C - \frac{1}{2} I^2 R - K \Delta T \quad (1)$$

$$Q_H = (\alpha_P - \alpha_N) I T_H + \frac{1}{2} I^2 R - K \Delta T \quad (2)$$

Table 1 Relevant parameters of Eqs. (1), (2)

T_C	T_H	α_p-α_n	K	ΔT
Absolute temperature on cold side	Absolute temperature on heat side	Sebeck coefficients between N-type and P-type	Thermal conductivity	Temperature variations between cold side and hot side
K	K	V/K	W/m.K	K

Consequently, based on Eqs. (1), (2), the internal relationship between Q_C and Q_H was deduced as shown in Eq. (3), which coupled with Eq. (4) of input power [25].

$$Q_H = Q_C + W \quad (3)$$

$$W = U.I = I^2 R + \alpha I \Delta T \quad (4)$$

Where *W, U, I* were the input power, the input voltage and the input current respectively. Considering actual processing temperature, the heating rate and cooling rate of the system were about 0.3°C/s and 0.1°C/s respectively. The Eq. (5) demonstrated theoretical heating/cooling power, and the Eq. (6) exhibited identification of TRR's numbers to be used. The related parameters of Eq. (5) and Eq. (6) were shown in the following table 2. $Q_{C/H}$ was the rated power of TRRs, and *n* was TRR's numbers.

$$Q_{c/h} = C_p . \rho . V . v_{c/h} \quad (5)$$

$$n \geq \frac{Q_{c/h}}{Q_{C/H}} \quad (6)$$

Table 2 Relevant parameters of Eqs. (5), (6)

C_P	ρ	v	$Q_{c/h}$	$v_{c/h}$
Specific heat capacity	Material density	Volume of pressing head plate	Total Heating/Refrigeration power	Heating/ Cooling rate
J/Kg.K	Kg/m^3	m^3	J/s	K/s

3 Design of the Hot embossing machine and initial boundary conditions

3.1 Frame structure and initial boundary conditions

In this paper, Closed frame structure with high stability consisted of the crossbeam, moving crossbeam, lower crossbeam and columns. The screw lift was connected to

the moving crossbeam by flange, and the feeding motion was achieved via the linear bearing motion pair. Dramatically, the lower crossbeam were able to achieve the free movement in the vertical direction, and the maintainability and replacement of pressure sensor installed on the bottom were accomplished with the characteristics of short time and easy operation. And the closed frame structure was shown in Figure 1.

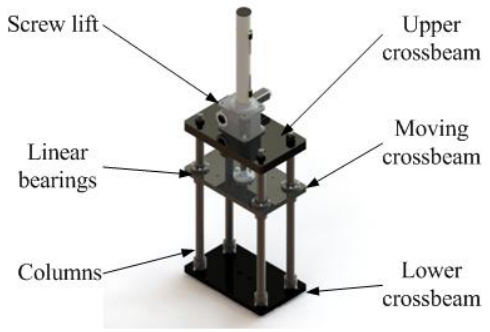

Figure 1 Structure of closed frame

To ensure fitting accuracy of the pressing heads, static simulation of columns as vertical moving guide was conducted, The radial stiffness of the column was studied in terms of material and size. The following were the specific simulation condition. Tetrahedral meshes were employed owing to simplicity of the model. Additionally, total loads of 3.1KN including the weight of the upper equipment and the pressing load were applied to the shoulder, and the fixed support was exerted to the bottom of the shaft. Parameters of sizes and grid were shown in table 3

Table 3 Relevant parameters of column

Material	*Length of shaft body*	*Diameter of body*	*Length of shaft head*	*Diameter of shoulder*	*Allow -able stress*
Aluminum alloy 6061	605mm	30mm	20mm	65mm	13.8 Mpa
Stainless steel 202	605mm	30mm	20mm	65mm	66.7 Mpa
Structure steel Q235	605mm	25/30/35 mm	20mm	65mm	58.7 Mpa

3.2 Structure of pressing head and initial boundary conditions

In this paper, the TRRs were utilized as heating/refrigerating unit, and separate pressing head was developed, which achieved the separation of the pressing load and the TRR's preload. Firstly, the parts of bearing pressing load were pressing head plate, heat insulating mattres, side beam, middle beam and lower slab. And the heat insulating mattres was used to reduce heat loss, and improve the heating efficiency. Secondly, the parts of applying TRR's preload was bolt, spring washer, rubber mat, cover of water tank, body of water tank, pad of TRR. The construction of pressing head was shown in Figure 2.

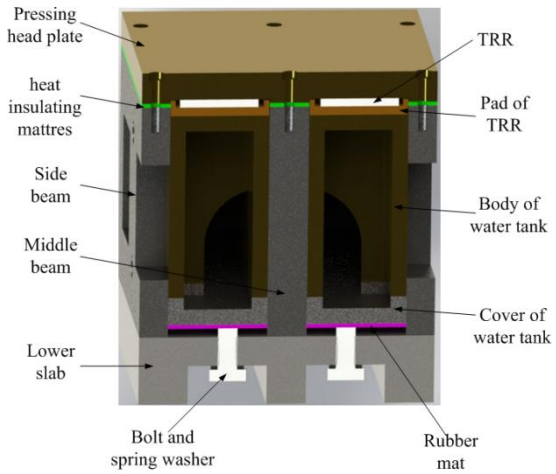

Figure 2 Structure of pressing head

In order to improve the force uniformity of the chip, three types of separate pressing heads were designed. And then, distributions of deformation on the feed direction were analysed for different types of pressing head as shown in Figure 3.

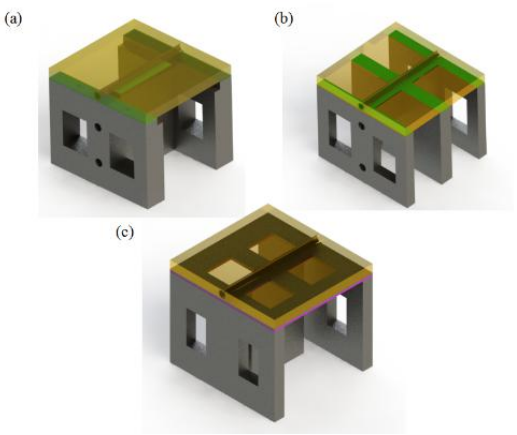

Figure 3 The three types (“工”，“王”，“田”) of separated head structure

The following were the specific simulation condition. Tetrahedral meshes were employed owing to the simplicity of the head structure. Because the size of the processing chip was 40mm*40mm*2mm, the working force of 2KN was applied to the central area of 40mm*40mm on the

surface of the head plate, and the fixed support was exerted to the bottom of beams. The related parameters of types were shown in table 4. And the simulation results were shown in the Figure 5.

Table 4 Simulation parameters of types of pressing heads

Types	*Overall Size*	*Head plate*	*Heat insulation*	Beam
Shape of "工"	150mm*160mm *140mm	brass	polycarbo nate	45 steel
Shape of "王"	150mm*160mm *140mm	brass	polycarbo nate	45 steel
Shape of "田"	150mm*160mm *140mm	brass	polycarbo nate	45 steel

3.3 Head plate and initial boundary conditions

To reduce thermal stress on accuracy of channel duplication of microfluidic chip, Force-thermal coupling simulation of pressing head plate as a core component was conducted, and effects of distributions of deformation and temperature were discussed.

Based on the Eqs. (4), (5), the TRR's number of four with a rated Q_C of 125w were selected. The thermal load was imposed on the TRR, and the working force of 2KN was applied to the central area of 40mm*40mm on the surface of the head plate, and the fixed support was exerted to the bottom of the beams. Simultaneously, tetrahedral meshes were adopted. For the given heat time of 300s, the parameters of numerical simulation were shown in table 5.

Table 5 Simulation parameters of head plate

Material	*Size*	*Thickness*	*Elements*	*Nodes*
Brass	150mm*160mm	14mm	25730	49835
Brass	150mm*160mm	16mm	19080	35802
Brass	150mm*160mm	18mm	13024	30058

4 Results and discussion

4.1 Simulation result and discussion of column

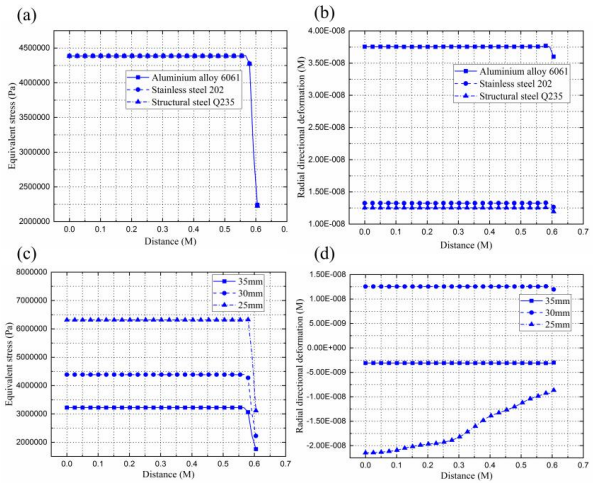

Figure 4 Simulation results of column

Through establishing the axial path on the column bottom's center, distributions of stress and stiffness for common materials were exhibited in Figure 4(a, b). Moreover, the general curve trends of the two graphs were similar. The stress curve changed slightly in the region of x<0.58m. Nevertheless, it declined with a large rate in the region of x>0.58m. The phenomenon was attributed to the fact that the total loads exerted to the shoulder resulted in a sharp change of the regional stress near the shoulder. Whereas the stress far from the shoulder area tended to be gentle. Apparently, the distribution of stress in Figure 4(a) were highly overlapped. Taking the point of x=0.58m as an example, the maximum stress is $4.6*10^6$Pa, and it was less than the corresponding allowable strength as shown in the table 3. Consequently, the strength requirement was satisfied. The obvious distinction among the radial deformation curves was demonstrated in Figure 4(b). For instance, when x=0.625m, the corresponding deformation of aluminum alloy, stainless steel, structural steel were $3.75*10^{-8}$m, $1.3*10^{-8}$m and $1.25*10^{-8}$m, respectively. The phenomenon was attributed to the fact that elastic modulus of 6061 was about 1/3 times than that of Q235 and 202, while the difference between Q235 and 202 was not significant.

Subsequently, the strength and stiffness of different sizes were investigated in Figure 4(c, d). On account of the same loads applied to the shoulder, the change trend was the first gentle and then sharp decline with the limit of x=0.58m. Furthermore, when x = 0.58 m, the maximum stresses of 25 mm, 30 mm and 35 mm were respectively $6.4*10^6$Pa, $4.4*10^6$Pa and $3.25*10^6$Pa. And the strength requirements were guaranteed, because the stress mentioned above were less than the corresponding allowable strength shown in

the table 3. Apparently, for the 25 mm column, the issue of the insufficient stiffness was exposed in the Figure 4(d). the stiffness of 30mm was not different from that of 35mm. and the distributions of deformation of 30nm and 35nm were homogeneous, which was able to improve the fitting accuracy of the pressing heads.

Moreover, in view of cost and fitting accuracy, the Q235 with the maximum stiffness was employed. and the size of 30mm is identified.

4.2 Simulation result and discussion of pressing head

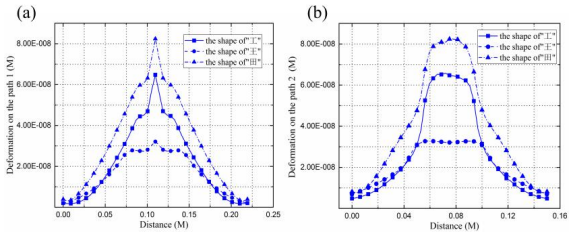

Figure 5 Simulation results of pressing head

In this paper, three types of head structures were designed as shown in Figure 3. Compared with the shapes of "工" and "王", the difficulty in installing TRR was increased via adopting the shape of "田". Through establishing diagonal line and central line of the pressing head plate as path 1 and path 2, distributions of deformation on the feed direction were demonstrated in the Figure 5(a,b). The overall trends in the two graphs were highly symmetrical on account of three symmetrical head structures. As the distance increased, Nodes on the path gradually passed through the central area locating in the application area of the working load. Consequently, that overall trend was firstly increasing and then decreasing. Different from the deformation distribution in Figure 5(b), the slope of the peak area in Figure 5(a) changed with a large rate. This phenomenon was attributed to the thickness change of the head plate. Taking x=0.11m as an example in Figure 5(a), the maximum deformation values of the shape of "工", the shape of "王" and the shape of "田" were respectively $8.1*10^{-8}$m, $6.5*10^{-8}$m and $3.2*10^{-8}$m. It was inferred that although the deformation range of the three structures reaches 10 nm, the average deformation of the shape of "王" was the best than that of the other types. Similarly, deformation curve in Figure 5(b) also confirmed that the mechanical properties of the "王"-type were super than those of the other structures. Consequently, through comprehensively considering the installation difficulty of TRR and the uniformity of deformation in the central region, the shape of "王" with the smallest deformation distribution was adopted.

4.3 Simulation result and discussion of pressing head plate

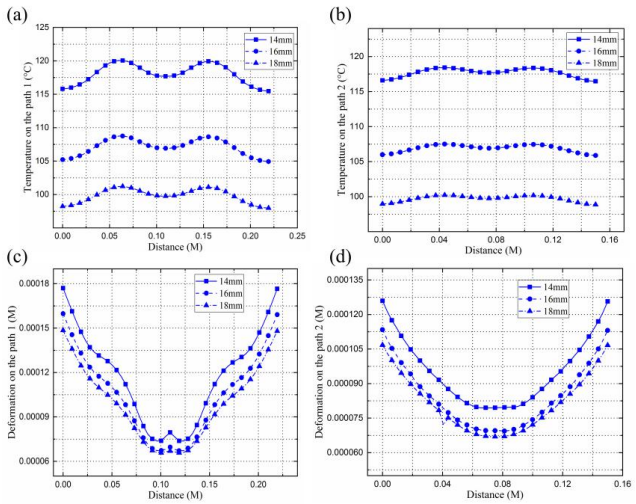

Figure 6 Simulation results of pressing head plate

For the given parameters including the shape of "王" and the heating time of 300s, through esablishing the diagonal and center line of the indenter plate as the path 1 and path 2, effects of distributions of deformation and temperature were discussed in Figure 6. because the TRRs were symmetrically installed under the pressing head plate, distribution of temperature on the two paths exhibited the shape of double hump with the highly symmetrical characteristic. Particularly, as the distance increased in the region of (x<0.11m), the path gradually passed through the installation area of the TRR, which induced to the temperature trend of firstly increasing and then decreasing. And then the first hump point (x=0.07m) appeared in the center of the TRR's installation. Additionally, because the middle beam induced to significant heat loss, the minimum temperature occured at x=0.11m. Apparently, the temperature distribution at x>0.11m was symmetric with the above region, which was not discussed here. Furthermore, with the decrease of thickness of head plate, the thermal capacity got smaller. And then the heating rate was improved under the same conditions. And it was confirmed that the average heating rate of 14mm, 16mm and 18mm were respectively 0.39°C/s, 0.35°C/s and 0.33°C/s.

Compared with the temperature distribution in Figure 6(a), the temperature variations of the corresponding three curves in Figure 6(b) were small, because the thickness of the head plate remains unchanged on the path 2.

Simultaneously, combining the temperature curves of the two paths, the temperature uniformity of the head plate for 14 mm was poor, while that of 16 mm was approximately consistent with that of 18mm. It was remarkable that uneven temperature distribution resulted in larger thermal stress, and ultimately affected processing accuracy of microchip. As a consequence, the size of 14mm don't satisfied the mentioned requirement in this paper.

And then to further reveal the deformation of the head plate with thermal load, the influence of deformation distribution were respectively plotted as shown in Figure 6(c, d). Obviously, the overall trend of deformation curve presented symmetrical shape of "W" in Figure 6(c). More specifically, as the increase of distance in the region of x<0.11m, the curve exhibited the decline trend with the appearance of inflection point at x=0.03m. it would be attributed to that the nodes located in direct acting area of TRR made the temperature nearby suddenly change. Additionally, due to the smallest thickness of the head plate, thermal expansion rate at the center (x=0.11m) was much lower than that at the edge, and thereby brought about the greatly changed peak slope. Apparently, the temperature distribution at x>0.11m was symmetric with the above region, which was not discussed here. Nevertheless, because the path 2 was always along the middle beam direction and does not pass through the installation area of TRR, the corresponding curve of deformation distribution in Figure 6(d) generally took the shape of "U", with no inflection point and minimum point.

Through combining with the distributions of deformation and temperature curves on path 1 and 2, the uniformity ratio of 16mm and 18mm were 0.07°C/um^2 and 0.03°C/um^2. Based on the comprehensive consideration of heating rate and thermal stress, the thickness of 16mm was identified.

5. Concluding Remarks

(1) the hot embossing machine composed of the frame structure and the pressing heads structure is established. The closed frame structure was employed and the screw drift was used to achieve feeding movement.
(2) According installation characteristic of TRR, the separate pressing head was established, which achieve which achieved the separation of the pressing load and the TRR's preload.
(3) Static simulation of columns as vertical moving guide was conducted, The simulation results demonstrate that the column with the material of Q235 and the size of 30mm possess sufficient strength and proper rigidity.
(4) Distributions of deformation on the feed direction were analysed. and pressing head of shape of "王" was employed with the character of easy installation of TRR and good uniformity of deformation.
(5) Force-thermal coupling simulation of pressing head plate as a core component was conducted. And the head plate of thickness of 18mm was adopted and it possessed the moderate heating rate and little thermal stress.
(6) the applied thermal load decreased deformation uniformity to a certain extent

7 Declaration

Acknowledgements

The authors sincerely thanks to Professor Junyao Wang of Northeast Electric Power University for his critical discussion and reading during manuscript preparation.

Funding

Supported by National Natural Science Foundation of China (Grant No. 51505077), Project Agreement for Science and Technology Development of Jilin Province (20170520099JH).

Availability of data and materials

The datasets supporting the conclusions of this article are included within the article.

Authors' contributions

The author' contributions are as follows: Qi Sun, Fu-wang Wang and Bo You were in charge of the design of hot embissing machine; Qi Sun wrote the manuscript; Junyao Wang assisted with simulation analyses.

Competing interests

The authors declare no competing financial interests.

Consent for publication

Not applicable

Ethics approval and consent to participate

Not applicable

References

[1] Wang Q , Liu W , Xing Y , et al. Screening of DNA Aptamers against Myoglobin Using a Positive and Negative Selection Units Integrated Microfluidic Chip and Its Biosensing Application[J].

Analytical Chemistry, 2014, 86(13): 6572-6579.
[2] Han J P, Sun J, Wang L, et al. The Optimization of Electrophoresis on a Glass Microfluidic Chip and its Application in Forensic Science[J]. *Journal of Forensic Science*s, 2017, 62(6): 1603-1612.
[3] Yeh C H, Lin P W, Lin Y C. Chitosan microfiber fabrication using a microfluidic chip and its application to cell cultures[J]. *Microfluidics & Nanofluidics*, 2010, 8(1): 115-121.
[4] Lee K G, Park T J, Song Y S, et al. Synthesis and utilization of E. coli-encapsulated PEG-based microdroplet using a microfluidic chip for biological application[J]. *Biotechnology & Bioengineering*, 2010, 107(4): 747-751.
[5] G. Romagnoli, D. Alvarez Feito, B. Brunel, et al. Silicon micro-fluidic cooling for NA62 GTK pixel detectors[J]. *Microelectronic Engineering*, 2015, 145(C): 133-137.
[6] Zoltán Fekete. Technology of ultralong deep brain fluidic microelectrodes combined with etching-before-grinding[J]. *Microsystem Technologies*, 2015, 21(2): 341-344.
[7] Luo, Chunxiong, Fu, Qiang, Li, Hao, et al. PDMS microfludic device for optical detection of protein immunoassay using gold nanoparticles[J]. *Lab on A Chip*, 5(7): 726.
[8] Chen J J , Shen C M , Ko Y W . Analytical study of a microfludic DNA amplification chip using water cooling effect[J]. *Biomedical Microdevices*, 2013, 15(2): 261-278.
[9] Martin P, Arben M, Salvador A. New materials for electrochemical sensing VII. Microfluidic chip platforms[J]. *Trac Trends in Analytical Chemistry*, 2006, 25(3): 219-235.
[10] Ren K, Zhou J, Wu H. Materials for microfluidic chip fabrication[J]. *Accounts of Chemical Research*, 2013, 46(11): 2396-2406.
[11] Ali A , Bao X Y , Qiao D , et al. Application of polymer materials in developing of slow control release fertilizers[J]. *Acta Polymerica Sinica*, 2015, 9(9): 1010-1019.
[12] Bar-Cohen, Yoseph. Current and future developments in artificial muscles using electroactive polymers[J]. *Expert Review of Medical Devices*, 2005, 2(6): 731-740.
[13] Yimge Juang, Lee L J, Koelling K W. Rheological analysis of polyvinyl butyral near the glass transition temperature[J]. *Polymer Engineering and Science*, 2001, 41(2): 275-292.
[14] Nam G J , Lee J W . Finite Element Analysis of the Effect of Processing Conditions on Thermoforming[J]. *Journal of Reinforced Plastics & Composites,* 1999, 18(7): 673-682.
[15] Kimerling T E , Liu W , Kim B H , et al. Rapid hot embossing of polymer microfeatures[J]. *Microsystem Technologies*, 2006, 12(8): 730-735.
[16] Shan X C, Ikehara T, Murakoshi Y, et al. Applications of micro hot embossing for optical switch formation[J]. *Sensors and Actuators A (Physical)*, 2005, 119(2): 433-440.
[17] Chang Y K, Hong F C N. The fabrication of Zn0 nanowire field-effect transistors combining dielectrophoresis and hot-pressing[J]. *Nanotechnology*, 2009, 20(23): 235202.
[18] Bae S , Kim H , Lee Y , et al. Roll-to-roll production of 30-inch graphene films for transparent electrodes[J]. *Nature Nanotechnology*, 2010, 5(8): 574-578.
[19] HE Yong, FU Jian zhong, CHEN Zi Chen. Temperature precise control in hot embossing device[J]. *Optics and Precision Engineering,* 2008, 16(5): 845-850.
[20] Xie D , Chang X , Shu X , et al. High Precision Temperature Control System for an Oven-Controlled Crystal Oscillator[J]. *The Open Automation and Control Systems Journal*, 2015, 7(1): 1690-1697.
[21] Wang X, Luo Y, Liu C, et al. Process Parameter Determination in Fabrication of Microchannel of Plastic (PMMA) Microfluidic Chips Using Hot-embossing Method[J]. *China Mechanical Engineering*, 2005, 16(22): 2061-2063.
[22] Yi L , Xiaodong W , Wang Liding, et al. Bonding Techniques for Fabrication of Thermoplastic Microfluidic Chips[J]. *China Mechanical Engineering*, 2008, 19(24):3012-3018.
[23] He Wei, Zhang Gan, Zhang Xingxing, et al. Recent development and application of thermoelectric generator and cooler[J]. *Applied Energy*, 2015, 143: 1-25.
[24] John Wiley, Sons Ltd. A comprehensive review of solar thermoelectric cooling systems[J]. *International Journal of Energy Research*, 2018, 48(2): 395-415.
[25] Jiang J , Chen L , Bai S , et al. Thermoelectric performance of p-type Bi－Sb－Te materials prepared by spark plasma sintering[J]. *Journal of Alloys and Compounds*, 2005, 390(1-2): 0-211.

Biographical notes

Jun-yao Wang, born in 1984. is currently a teacher in *school of mechanical engineering of Northeast Electric Power University*. He received his PhD degree from *Dalian Jiaotong Universityy, China*. His research interests include micro-nano fabrication and micro-nano fluids.
Tel: +86-15981176407; E-mail: junyao_0001@126.com

Qi Sun, born in 1993, is currently a master candidate at *Northeast Electric Power University, China*. He received his bachelor degree from *Shandong University of Technology, China*, in 2017.
G-mail: 1171470526@qq.com

Bo You, born in 1983. is a teacher in *school of mechanical engineering of Jilin University of Chemical Technology*. He received his PhD degree from *Dalian Jiaotong Universityy, China*. His research interests include precision press fitting and automation of small parts.
E-mail:youbo198362@163.com

Fu-wang Wang, born in 1981, is a teacher in *school of mechanical engineering of Northeast Electric Power University*. He received his PhD degree from *Dalian Jiaotong Universityy, China*. His research interests include EEG robot.
E-mail: wangfuwangbaiyang@126.com.

Figures

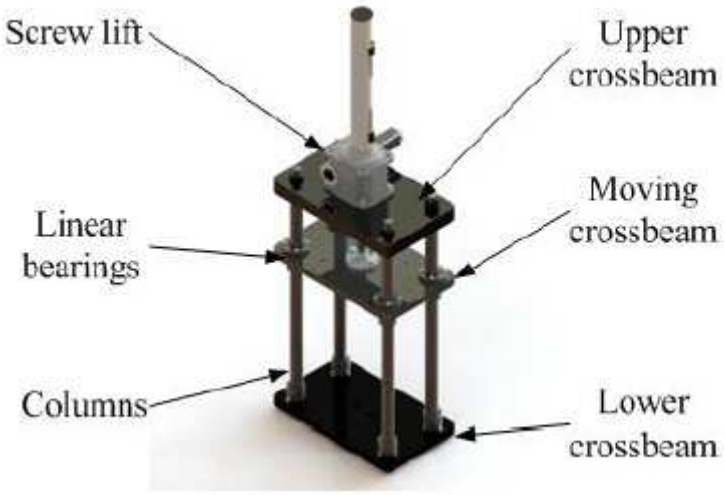

Figure 1

Structure of closed frame

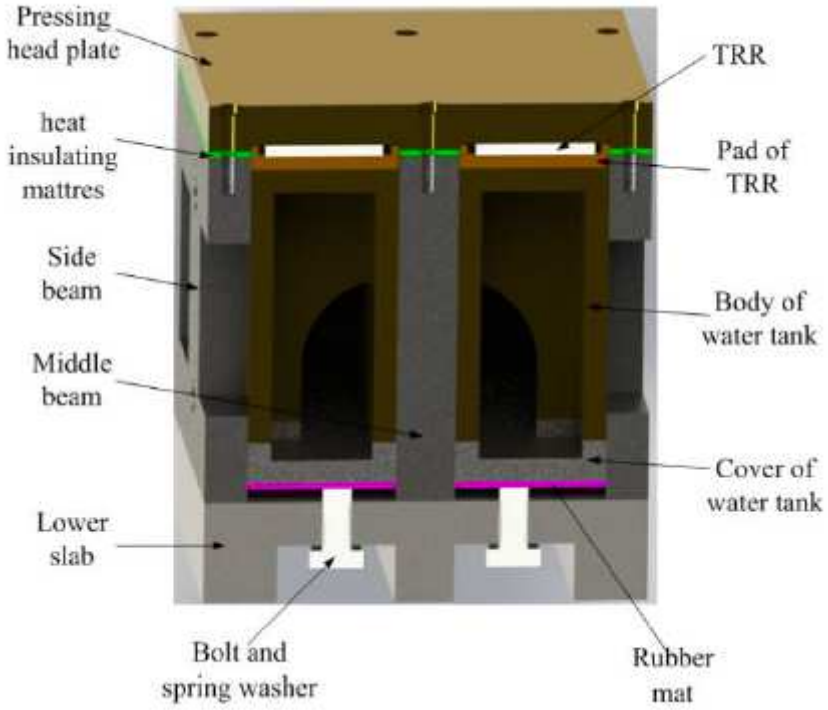

Figure 2

Structure of pressing head

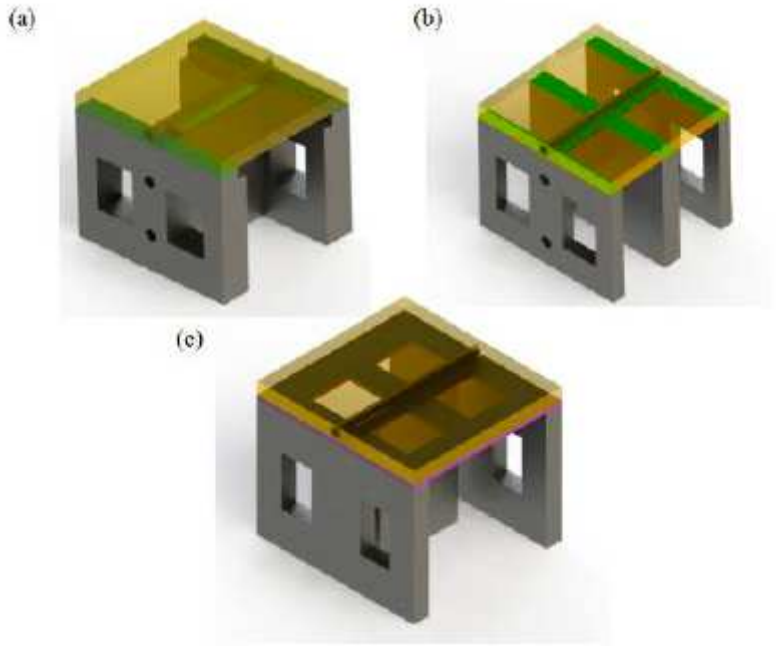

Figure 3

The three types (“□”□“□”□“□”) of separated head structure

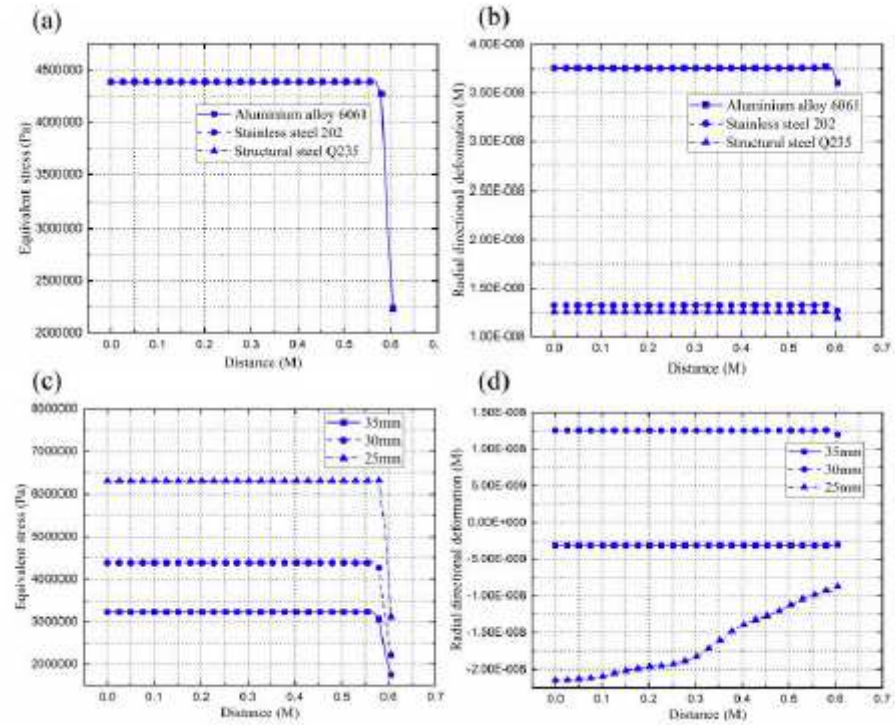

Figure 4

Simulation results of column

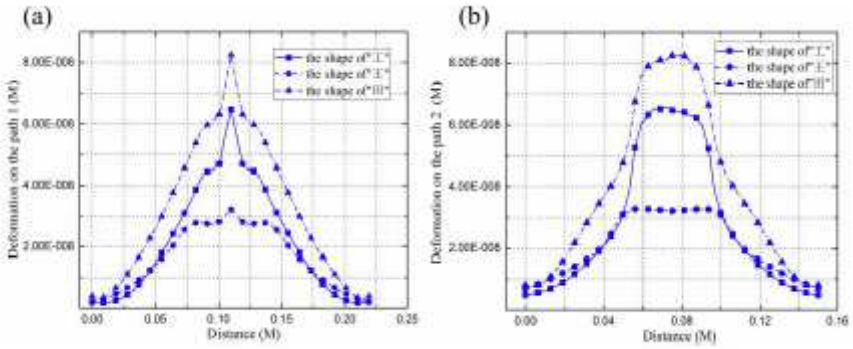

Figure 5

Simulation results of pressing head

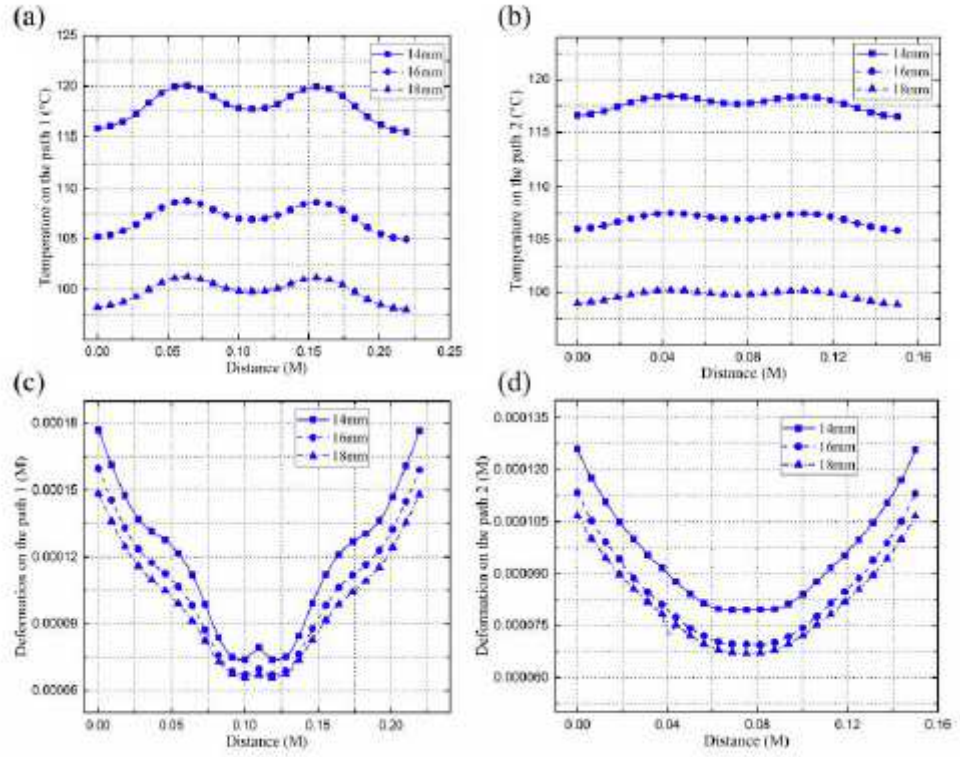

Figure 6

Simulation results of pressing head plate